

Statistic-Augmented, Decoupled MoE Routing and Aggregating in Autonomous Driving

Wei-Bin Kou^{1,2,3}, Guangxu Zhu³, Jingreng Lei¹, Chen Zhang¹, and Yik-Chung Wu^{1,*}, Jianping Wang^{2,*}

Abstract—Autonomous driving (AD) scenarios are inherently complex and diverse, posing significant challenges for a single deep learning model to effectively cover all possible conditions, such as varying weather, traffic densities, and road types. Large Model (LM)-Driven Mixture of Experts (MoE) paradigm offers a promising solution, where LM serves as the backbone to extract latent features while MoE serves as the downstream head to dynamically select and aggregate specialized experts to adapt to different scenarios. However, routing and aggregating in MoE face intrinsic challenges, including imprecise expert selection due to flawed routing strategy and inefficient expert aggregation leading to suboptimal prediction. To address these issues, we propose a statistic-augmented, decoupled MoE Routing and Aggregating Mechanism (MoE-RAM) driven by LM. Specifically, on the one hand, MoE-RAM enhances expert routing by incorporating statistical retrieval mechanism to match LM-extracted latent features with cached prototypical features of the most relevant experts; on the other hand, MoE-RAM adaptively reweights experts' outputs in fusion by measuring statistical distances of experts' instant features against LM-extracted latent features. Benefiting from the synergy of the statistic-augmented MoE's routing and aggregating, MoE-RAM ultimately improves the prediction performance. We take the AD semantic segmentation task as an example to assess the proposed MoE-RAM. Extensive experiments on AD datasets demonstrate the superiority of MoE-RAM compared to other MoE baselines and conventional single-model approaches.

I. INTRODUCTION

Autonomous driving (AD) stands at the forefront of artificial intelligence applications, demanding models that can process and respond to an extraordinarily diverse real-world scenarios in real time [1]–[5]. These scenarios encompass a broad spectrum of complexities [6]–[8], including but not limited to dense urban traffic with unpredictable pedestrian movements, high-speed highway navigation under varying lighting conditions, rural roads with irregular terrains, and adverse weather conditions such as heavy rain, fog, or snow that obscure sensor inputs [9]. The inherent variability in these environments poses a fundamental limitation for a single deep learning model. Such models often overfit to dominant patterns in training data, failing to generalize to

edge cases or unseen situations, which can result in critical safety risks in AD.

Large Model (LM)-Driven Mixture of Experts (MoE) [10]–[13] paradigm emerges as an promising solution to tackle these AD shortcomings. Specifically, a pretrained LM serves as the backbone to extract latent features of input, while multiple parallel fine-tuned "experts" (*i.e.*, MoE) collectively serve as the downstream head to conduct relevant tasks, such as object detection, semantic segmentation, etc. In general, a routing (aggregating) mechanism dynamically selects (aggregates) the most relevant experts based on the input. However, the AD-oriented MoEs are hampered by their inherent challenges in routing and aggregating. First, existing MoE routing mechanisms typically rely on gating functions [14], [15] (e.g., softmax-based functions) which are sensitive to feature mismatches. In dynamic AD environments, these routing functions often fail to accurately map inputs to the optimal experts, leading to suboptimal prediction accuracy. Second, inefficient aggregation compounds MoE's prediction performance, as conventional methods (e.g., simple weighted averaging) do not adequately capture inter-expert statistical dependencies, resulting in underestimated fusion activations. This inefficiency is particularly pronounced in non-IID (non-independent and identically distributed) AD scenarios.

To mitigate these challenges in MoE routing and aggregating and further consolidate MoE in AD application, we propose a novel LM-Driven MoE framework with statistic-augmented, decoupled Routing and Aggregating Mechanism (MoE-RAM). Specifically, MoE-RAM comprises following integral components: (I) Pretrained ViT Backbone: we propose to use a pretrained Vision Transformer (ViT) as the backbone to extract latent features of each sensory image, which serve as the input of the downstream MoE architecture. (II) Downstream MoE with Expert-Wise Feature Retrieval Library (FRL): following the pretrained ViT backbone, we propose to deploy multiple CNN experts parallelly to form the MoE architecture to serve as the downstream task head. Each expert contains a FRL to store itself prototypical feature patterns, which represent individual expert's expertise and knowledge. FRL is updated by a read-then-update manner by using attention-based method. (III) Statistical Retrieval-Augmented MoE Routing Mechanism (MoE-RM): we enhance the MoE routing process by integrating a retrieval mechanism that statistically queries each expert's FRL to identify the most relevant experts. This is achieved through measuring Jensen-Shannon divergence to align ViT-

*Corresponding author: Yik-Chung Wu (ycwu@eee.hku.hk) and Jianping Wang (jianwang@cityu.edu.hk).

¹Department of Electrical and Electronic Engineering, The University of Hong Kong, Hong Kong 999077, China.

²Department of Computer Science, City University of Hong Kong, Hong Kong 999077, China.

³Shenzhen International Center For Industrial And Applied Mathematics, Shenzhen Research Institute of Big Data, Shenzhen, China.

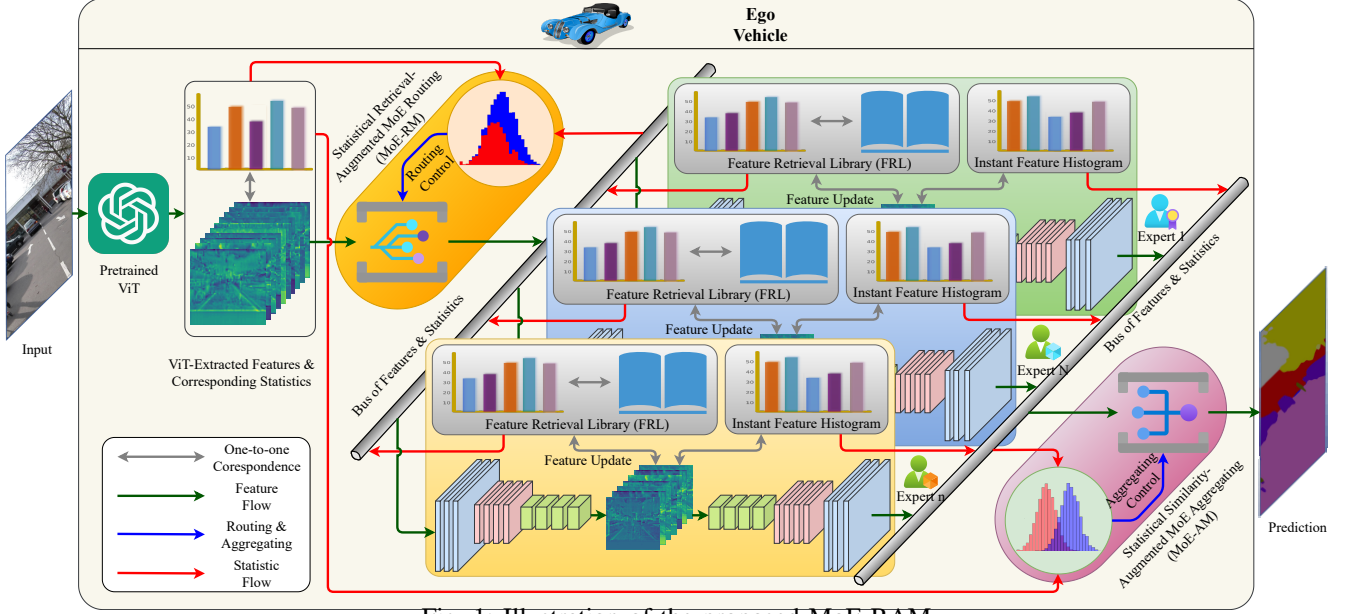


Fig. 1: Illustration of the proposed MoE-RAM.

extracted latent features with each expert expertise in itself FRL, enabling precise, scenario-aware expert selection. For example, in a foggy driving scenario, MoE-RM retrieves experts who specialize in low-visibility driving scenario's prediction, ensuring adaptive and accurate prediction. (IV) Statistical Similarity-Augmented MoE Aggregating Mechanism (MoE-AM): to overcome the flawed experts' fusion policy, we propose a statistical similarity-based expert aggregation mechanism that employs dynamic statistical reweighting scheme, which aggregates expert outputs by considering their statistical distribution alignments. Specifically, we firstly calculate statistical distances of all experts' instant features against ViT-extracted latent features using Jensen-Shannon divergence; we then assign aggregation weight for each expert by computing the proportion of its distance reciprocal relative to the total sum of distance reciprocal of all experts.

By synergistically integrating abovementioned routing and aggregating mechanisms (*i.e.*, MoE-RM and MoE-AM), the proposed MoE-RAM transforms MoE into a more robust and intelligent system, tailored to the AD demands where precision and adaptability are paramount. The proposed MoE-RAM is illustrated in Fig. 1. We take the AD semantic segmentation task as an example to evaluate the proposed MoE-RAM. Extensive experiments on AD benchmarks demonstrate that the proposed MoE-RAM outperforms other MoE baselines and single-model competitors.

Main contributions of this work are highlighted as follows:

- MoE routing and aggregating generally impair the prediction accuracy for AD-oriented MoE systems. To mitigate this issue, we propose MoE-RAM to enhance the routing and aggregating of MoE from statistic perspective. The proposed MoE-RAM comprises a pretrained ViT backbone, expert-wise FRLs, a statistical retrieval-augmented MoE routing mechanism (*i.e.*, MoE-RM), and a statistical similarity-augmented MoE aggregating

mechanism (*i.e.*, MoE-AM).

- Expert-wise FRLs are updated in a read-then-update fashion based on attention mechanism to store experts' expertise and knowledge. MoE-RM deploys both the retrieved experts' statistic from respective FRL and ViT-extracted features' statistic to determine which subset of experts is selected. MoE-AM dynamically assigns weights for involved experts in MoE aggregation, which is achieved by measuring statistical alignment of participated experts' features with the ViT-extracted features.
- Extensive experiments on AD datasets show that the proposed MoE-RAM outperforms other MoE baselines and single-model competitors in prediction accuracy.

II. RELATED WORK

A. Foundation Models Towards AD

Recent advancements in Large Language Models (LLMs), such as the GPT [16] and LLaMA [17], have revolutionized natural language processing. Similarly, models such as LLaVA [18], ShareGPT4V [19] integrate visual information to enable tasks like image captioning and visual question answering. These Vision-Language Models (VLMs) are typically trained on extensive image-text datasets [20]. Early VLMs focused on static images [21], but recent efforts have extended their capabilities to video understanding such as Qwen2-VL [22], incorporating temporal dynamics into the language feature space for sequence comprehension. Several recent works explore the potential of VLMs for AD [23]. For example, Dolphins [24] employs Visual Question Answering (VQA) to bridge the gap between data-driven driving and user trust. Besides, decision-making and planning are also being integrated into VLMs, as seen in DriveVLM [25] and Reason2drive [26], where the training data is always divided into perception, prediction, and planning components. These models often produce outputs, including scene descriptions, action analysis, hierarchical planning, etc. End-to-end AD

approaches such as DriveGPT4 [27] and LMDrive [28] attempt to directly map visual and linguistic inputs to planning or low-level control signals.

B. Mixture of Experts (MoE) Towards AD

The MoE architecture has emerged as a pivotal method for scaling LMs and enhancing task specialization. By employing MoE designs, model capacity and processing efficiency are significantly improved [10]. The primary strength of MoE lies in its ability to harness the specialization of individual experts across diverse data, thereby boosting overall model performance. For instance, [11] applies a task-level MoE to multilingual translation, routing inputs intelligently based on task identifiers, resulting in notable performance gains and improved inference efficiency. While MoE has shown great promise in LLMs and VLMs, its application in AD remains relatively underexplored. Existing studies have examined MoE architectures in AD for specific tasks, such as rare scenario perception [12], long-tailed trajectory prediction [13], domain adaptation under varying weather conditions [29], safe trajectory prediction and planning [30], and generalization of planners [31]. However, these approaches have yet to fully exploit MoE’s potential to deliver adaptive and robust performance across diverse and complex AD scenarios.

C. MoE’s Routing and Aggregating

MoE routing is generally achieved through a gating function that assigns inputs to preferred experts based on specific criteria. Linear gating functions [32], [33], such as softmax-based gating, are commonly used due to their simplicity and effectiveness. These functions compute a probability distribution over experts and often include a TopK operation to select the top-k experts. Non-linear alternatives [14], [34] such as cosine similarity-based gating have been introduced to enhance generalization. These approaches generally project inputs into a hyperspherical space and compare them to expert embeddings. SoftMoE [15] explore exponential family distributions for weighted averaging to avoid discrete token dropping. MoE aggregation combines the outputs of selected experts by weighted summation, where weights are determined by the gating function. For example, the output of Transformer-based MoE is calculated as a linear combination of the outputs of feed-forward networks (FFNs) of all selected experts [32]. Variants such as mixture-of-attention (MoA) [35] dynamically aggregate attention heads. These aggregation mechanisms ensure efficient knowledge integration while addressing challenges such as load imbalance through auxiliary loss functions. In this paper, we consider the MoE’s routing and aggregating separately from statistical perspective, and decouple the inter-dependency of MoE’s routing and aggregating, aiming at enhancing MoE’s overall prediction performance.

III. METHODOLOGY

The proposed MoE-RAM is composed of a pretrained ViT backbone, expert-wise FRLs, a statistical retrieval-

TABLE I: Key Notations in MoE-RAM

Notation	Explanation
\mathcal{D}	Dataset of RGB images.
$\mathcal{D}^{(i)}$	The i -th input RGB image of \mathcal{D} .
ω_{ViT}	Parameters of the pretrained ViT backbone.
$\mathcal{F}_{ViT}^{(i)}$	ViT-extracted latent features of $\mathcal{D}^{(i)}$.
N	Number of experts in MoE.
\mathcal{E}_j, θ_j	The j -th CNN expert and its parameters.
$\mathcal{E}_j^{\text{enc}}, \theta_j^{\text{enc}}$	Encoder of expert j and its parameters (former part of \mathcal{E}_j).
$\mathbf{h}_j^{(i)}$	Intermediate representations of expert j for input i .
$\mathbf{y}_j^{(i)}$	Task-specific output of expert j for input i .
\mathcal{M}_j	Feature Retrieval Library (FRL) of expert j .
K_j	Number of prototype entries in \mathcal{M}_j .
$\mathbf{p}_{j,k} \in \mathbb{R}^d$	The k -th prototype vector in expert j ’s FRL.
$w_{j,k} \geq 0$	Importance weight associated with prototype $\mathbf{p}_{j,k}$.
$\alpha_{j,k}^{(i)}$	Attention weight on prototype $\mathbf{p}_{j,k}$ for input i .
$\tilde{\mathbf{p}}_j^{(i)}$	Retrieved prototype from expert j for input i .
η	FRL memory update rate for read-then-update.
$Q^{(i)}$	Input-induced normalized distribution from $\mathcal{F}_{ViT}^{(i)}$.
$P_j^{(i)}$	Prototype-induced normalized distribution from $\tilde{\mathbf{p}}_j^{(i)}$.
$R_j^{(i)}$	Output-induced normalized distribution from $\mathbf{h}_j^{(i)}$.
$s_j^{(i)}$	Routing score for expert j on input i .
$\pi_j^{(i)}$	Routing probability for expert j on input i .
$\mathcal{S}^{(i)}$	Index set of TopK selected experts for input i .
$\delta_j^{(i)}$	JS divergence between $Q^{(i)}$ and $R_j^{(i)}$.
$\tilde{w}_j^{(i)}$	Reciprocal distance weight $1/(\epsilon + \delta_j^{(i)})$ for aggregation.
$\beta_j^{(i)}$	Aggregation weight for expert j , normalized over $j \in \mathcal{S}^{(i)}$.
$\hat{\mathbf{y}}^{(i)}$	Final aggregated output for input i .
B	Mini-batch size.

augmented routing mechanism MoE-RM, and a statistical similarity-augmented aggregating mechanism MoE-AM. They are introduced in Section III-A, Section III-B, Section III-C, and Section III-D, respectively. Finally, we detail the overall training objective of MoE-RAM in Section III-E.

A. Pretrained ViT Backbone

Pretrained ViT [36] is a widely used representation extractor to extract latent features of RGB data. Therefore, in this work, we, as usual, select ViT as the LM backbone (with parameters ω_{ViT}) to extract the latent features of inputs.

We denote the i -th input RGB image as $\mathcal{D}^{(i)}$ for dataset \mathcal{D} , and its latent features $\mathcal{F}_{ViT}^{(i)}$ is extracted in a zero-shot manner as follow

$$\mathcal{F}_{ViT}^{(i)} = \omega_{ViT}(\mathcal{D}^{(i)}), \quad (1)$$

where $\mathcal{F}_{ViT}^{(i)}$ is a high-dimensional tensor, representing the ViT’s understanding of the content of input $\mathcal{D}^{(i)}$.

B. Expert-Wise Feature Retrieval Library (FRL)

Following the pretrained ViT backbone, we deploy a downstream sparse MoE head composed of N parallel CNN experts $\{\mathcal{E}_j\}_{j=1}^N$, each parameterized by θ_j . To explicitly encode and preserve each expert’s specialization and expertise, we equip every expert \mathcal{E}_j with a Feature Retrieval Library (FRL) denoted as \mathcal{M}_j . The FRL stores prototypical feature patterns that summarize the expert’s learned expertise and scenario-specific knowledge.

Given the ViT-extracted latent feature $\mathcal{F}_{ViT}^{(i)}$ from Eq. (1), expert \mathcal{E}_j produces an intermediate representation $\mathbf{h}_j^{(i)}$ and a task-specific output $\mathbf{y}_j^{(i)}$:

$$\mathbf{h}_j^{(i)} = \mathcal{E}_j^{\text{enc}}(\mathcal{F}_{ViT}^{(i)}; \boldsymbol{\theta}_j^{\text{enc}}), \quad (2)$$

$$\mathbf{y}_j^{(i)} = \mathcal{E}_j(\mathcal{F}_{ViT}^{(i)}; \boldsymbol{\theta}_j), \quad (3)$$

where $\mathcal{E}_j^{\text{enc}}$ is the expert-embedded encoder producing an expert-level representation $\mathbf{h}_j^{(i)}$ for updating FRL, and noting that $\mathcal{E}_j^{\text{enc}}$ is the former part of \mathcal{E}_j (i.e., $\boldsymbol{\theta}_j^{\text{enc}} \in \boldsymbol{\theta}_j$).

With respect to FRL of expert \mathcal{E}_j , \mathcal{M}_j is a set of K_j prototypical feature entries $\{(\mathbf{p}_{j,k}, w_{j,k})\}_{k=1}^{K_j}$ with vectors $\mathbf{p}_{j,k} \in \mathbb{R}^d$ and associated nonnegative importance weights $w_{j,k}$. We firstly compute attention weights $\alpha_{j,k}^{(i)}$ over \mathcal{M}_j to read expert prototypes $\mathbf{p}_{j,k}$ relevant to $\mathcal{F}_{ViT}^{(i)}$:

$$\alpha_{j,k}^{(i)} = \frac{\exp(\text{sim}(\mathcal{F}_{ViT}^{(i)}, \mathbf{p}_{j,k}))}{\sum_{\ell=1}^{K_j} \exp(\text{sim}(\mathcal{F}_{ViT}^{(i)}, \mathbf{p}_{j,\ell}))}, \quad (4)$$

$$\tilde{\mathbf{p}}_j^{(i)} = \sum_{k=1}^{K_j} \alpha_{j,k}^{(i)} \mathbf{p}_{j,k}, \quad (5)$$

where $\text{sim}(\cdot, \cdot)$ is a similarity function (e.g., cosine similarity), $\tilde{\mathbf{p}}_j^{(i)}$ is the retrieved prototype of expert \mathcal{E}_j for input $\mathcal{D}^{(i)}$, serving the role of expert selection in MoE routing.

Parallel with the forward pass, we perform a read-then-update step to adaptively refine \mathcal{M}_j as follows:

$$\mathbf{p}_{j,k} \leftarrow (1 - \eta \alpha_{j,k}^{(i)}) \mathbf{p}_{j,k} + \eta \alpha_{j,k}^{(i)} \psi_j(\mathbf{h}_j^{(i)}), \quad (6)$$

$$w_{j,k} \leftarrow (1 - \eta \alpha_{j,k}^{(i)}) w_{j,k} + \eta \alpha_{j,k}^{(i)}, \quad (7)$$

where η is a memory update rate and $\psi_j(\cdot)$ maps the experts' intermediate features into the prototype space. This attention-weighted update maintains compact, scenario-aware prototypes that reflect the expert's evolving competence.

C. Statistic-Augmented MoE Routing (MoE-RM)

To achieve precise, scenario-aware expert selection, we augment routing with statistical retrieval over FRLs. For expert \mathcal{E}_j , we estimate a prototype-induced distribution $P_j^{(i)}$ from $\tilde{\mathbf{p}}_j^{(i)}$, and then align it to the input-induced distribution $Q^{(i)}$ from $\mathcal{F}_{ViT}^{(i)}$ using Jensen–Shannon (JS) divergence:

$$Q^{(i)} = \text{Norm}(\mathcal{F}_{ViT}^{(i)}), \quad (8)$$

$$P_j^{(i)} = \text{Norm}(\tilde{\mathbf{p}}_j^{(i)}), \quad (9)$$

$$D_{\text{JS}}(Q^{(i)} \| P_j^{(i)}) = \frac{1}{2} (D_{\text{KL}}(Q^{(i)} \| I_j^{(i)}) + D_{\text{KL}}(P_j^{(i)} \| I_j^{(i)})), \quad (10)$$

where $\text{Norm}(\cdot)$ denotes a feature-to-distribution normalization (e.g., softmax over channels or bins), $D_{\text{KL}}(\cdot \| \cdot)$ is the Kullback–Leibler divergence, and $I_j^{(i)} = \frac{1}{2}(Q^{(i)} + P_j^{(i)})$.

We convert JS divergences into routing scores and probabilities based on following equations:

$$s_j^{(i)} = 1/(\epsilon + D_{\text{JS}}(Q^{(i)} \| P_j^{(i)})), \quad (11)$$

$$\pi_j^{(i)} = \exp(\tau s_j^{(i)}) / (\sum_{\ell=1}^N \exp(\tau s_{\ell}^{(i)})), \quad (12)$$

with small $\epsilon > 0$ for numerical stability and temperature $\tau > 0$ to control sharpness. Based on above scores, we

apply TopK routing to $\{\pi_j^{(i)}\}_{j=1}^N$. The routed set $\mathcal{S}^{(i)} \subseteq \{1, \dots, N\}$ contains the indices of selected experts for input $\mathcal{D}^{(i)}$.

Intuitively, experts whose FRLs better match the current scenario (lower JS divergence) receive higher routing probabilities. For instance, under foggy scenes, experts with FRLs encoding low-visibility patterns are prioritized by MoE-RM.

D. Statistic-Augmented MoE Aggregating (MoE-AM)

To address suboptimal fusion of expert outputs, we propose a statistical similarity-based aggregation that dynamically reweights experts in fusion according to expert \mathcal{E}_j 's intermediate representation $\mathbf{h}_j^{(i)}$'s distribution alignment with that of $\mathcal{F}_{ViT}^{(i)}$.

Given per-expert intermediate representation $\{\mathbf{h}_j^{(i)}\}_{j=1}^N$ for $j \in \mathcal{S}^{(i)}$, we firstly compute intermediate representation-induced distributions $R_j^{(i)}$ over $\mathbf{h}_j^{(i)}$ and measure their JS divergence to input-induced distribution $Q^{(i)}$ over $\mathcal{F}_{ViT}^{(i)}$:

$$R_j^{(i)} = \text{Norm}(\mathbf{h}_j^{(i)}), \quad j \in \mathcal{S}^{(i)}, \quad (13)$$

$$\delta_j^{(i)} = D_{\text{JS}}(Q^{(i)} \| R_j^{(i)}), \quad j \in \mathcal{S}^{(i)}. \quad (14)$$

We subsequently define a reciprocal-distance weight and normalize across the routed experts as below equations:

$$\tilde{w}_j^{(i)} = 1/(\epsilon + \delta_j^{(i)}), \quad j \in \mathcal{S}^{(i)}, \quad (15)$$

$$\beta_j^{(i)} = \tilde{w}_j^{(i)} / (\sum_{\ell \in \mathcal{S}^{(i)}} \tilde{w}_{\ell}^{(i)}), \quad j \in \mathcal{S}^{(i)}. \quad (16)$$

Finally, we aggregate outputs of routed experts with above statistical reweighting coefficient, i.e.,

$$\hat{\mathbf{y}}^{(i)} = \sum_{j \in \mathcal{S}^{(i)}} \beta_j^{(i)} \mathbf{y}_j^{(i)}. \quad (17)$$

This aggregation emphasizes experts whose outputs are distributionally consistent with the ViT-extracted latent features, providing adaptive, robust fusion under diverse, complex AD scenarios.

E. MoE-RAM's Overall Training Objective

MoE-RAM can be trained in an end-to-end manner. In this work, we take the AD semantic segmentation task as an example to evaluate the proposed MoE-RAM. The overall training objective comprises three parts: the standard cross entropy loss \mathcal{L}_{CE} , the MoE auxiliary load-balancing term \mathcal{L}_{LB} , and FRL regularizer \mathcal{L}_{FRL} . Thus, the overall training objective \mathcal{L} can be formulated as

$$\mathcal{L} = \mathcal{L}_{\text{CE}} + \lambda_{\text{LB}} \mathcal{L}_{\text{LB}} + \lambda_{\text{FRL}} \mathcal{L}_{\text{FRL}}, \quad (18)$$

where $\lambda_{\text{LB}}, \lambda_{\text{FRL}} \geq 0$ control regularization strengths. In the proposed MoE-RAM, term \mathcal{L}_{LB} is introduced to avoid expert collapse in training by pushing experts routed uniformly, and is defined as

$$\mathcal{L}_{\text{LB}} = \sum_{j=1}^N u_j \log u_j - \log N, \quad (19)$$

where $u_j = \frac{1}{B} \sum_{i=1}^B \pi_j^{(i)}$, $j = 1, \dots, N$. $\sum_{j=1}^N u_j \log u_j$ (minimized when $\{u_j\}_{j=1}^N$ is uniform) pushes to distribute traffic across all experts, avoiding expert collapse. Adding

Algorithm 1: MoE-RAM

Input: Dataset \mathcal{D} ; pretrained ω_{ViT} ; experts $\{\mathcal{E}_j\}_{j=1}^N$ with params $\{\theta_j\}_{j=1}^N$; FRLs $\{\mathcal{M}_j\}_{j=1}^N$ with $\{(\mathbf{p}_{j,k}, w_{j,k})\}_{k=1}^{K_j}$; update rate η ; temperature τ ; stability ϵ ; loss weights $\lambda_{\text{LB}}, \lambda_{\text{FRL}}$.

Output: Trained $\{\theta_j\}_{j=1}^N$, and updated $\{\mathcal{M}_j\}_{j=1}^N$.

Init: Initialize experts $\{\theta_j\}_{j=1}^N$; initialize $\{\mathcal{M}_j\}_{j=1}^N$ with $\mathbf{p}_{j,k} \in \mathbb{R}^d$ and weights $w_{j,k} \geq 0$.

```

1 for each training step do
2   Sample a mini-batch  $\{\mathcal{D}^{(i)}\}_{i=1}^B$  with labels;
   // 1) Backbone feature extraction
3   for  $i \leftarrow 1$  to  $B$  do
4      $\mathcal{F}_{\text{ViT}}^{(i)} \leftarrow \omega_{\text{ViT}}(\mathcal{D}^{(i)})$ ,  $Q^{(i)} \leftarrow \text{Norm}(\mathcal{F}_{\text{ViT}}^{(i)})$ 
   // 2) FRL retrieval per expert
5   for  $j \leftarrow 1$  to  $N$  do
6     for  $i \leftarrow 1$  to  $B$  do
7        $\alpha_{j,k}^{(i)}, \tilde{\mathbf{p}}_j^{(i)}, P_j^{(i)} \leftarrow \text{Eqs. (4), (5) and (9)}$ 
   // 3) Expert Routing
8   for  $i \leftarrow 1$  to  $B$  do
9      $\pi_j^{(i)} \leftarrow \text{Eq. (12)}$ ,  $\mathcal{S}^{(i)} \leftarrow \text{Top-}K(\{\pi_j^{(i)}\}_{j=1}^N)$ 
   // 4) Expert forward & aggregation
10  for  $i \leftarrow 1$  to  $B$  do
11    foreach  $j \in \mathcal{S}^{(i)}$  do
12       $\mathbf{h}_j^{(i)}, \mathbf{y}_j^{(i)}, R_j^{(i)}, \delta_j^{(i)} \leftarrow \text{Eqs. (2), (3), (13)}$ 
      and (14)
13       $\tilde{w}_j^{(i)}, \beta_j^{(i)}, \hat{\mathbf{y}}^{(i)} \leftarrow \text{Eqs. (15) to (17)}$ 
   // 5) Optimization Losses
14   $\mathcal{L}_{\text{LB}}, \mathcal{L}_{\text{FRL}}, \mathcal{L} \leftarrow \text{Eqs. (18) to (20)}$ 
   // 6) FRL read-then-update
15  for  $j \leftarrow 1$  to  $N$  do
16    for  $k \leftarrow 1$  to  $K_j$  do
17       $\mathbf{p}_{j,k} \leftarrow \text{Eq. (6)}$ 
   // 7) Parameter update
18  Update  $\{\theta_j\}_{j=1}^N$  with an optimizer step on  $\mathcal{L}$ .
```

$-\log N$ just zero-centers at the optimum. For the FRL regularizer \mathcal{L}_{FRL} , we propose to formulate it as

$$\mathcal{L}_{\text{FRL}} = \sum_{j=1}^N \sum_{k=1}^{K_j} (\underbrace{\|\mathbf{p}_{j,k}\|_2^2 + w_{j,k}^2}_{\text{Norm/Weight Decay}} + \underbrace{\sum_{i=1}^B |\alpha_{j,k}^{(i)}|}_{\text{Sparse Attention}}), \quad (20)$$

where *Norm/Weight Decay* prevents unbounded growth of prototype vectors and their importance scalars, controlling scale and avoiding trivial wins by increasing magnitude, and *Sparse Attention* over prototypes encourages the retriever to pick a few relevant prototypes rather than averaging many, which keeps retrieved signals sharp and interpretable.

In conclusion, the proposed MoE-RAM is outlined in Algorithm 1.

IV. EXPERIMENTS

In this section, we carry out comprehensive experiments to verify MoE-RAM on AD semantic segmentation task.

Specifically, we firstly introduce the experimental setup in Section IV-A. Subsequently, we conduct experimental comparison and related analyses in Section IV-B. We then visualize the relationship between ViT-extracted features and expert-wise FRL prototypes in Section IV-C. Finally, we conduct ablation studies to investigate various hyperparameters' effect on MoE-RAM's overall performance in Section IV-D.

A. Datasets, Evaluation Metrics and Implementation

1) *Datasets*: The **Cityscapes** dataset [37] includes 2,975 training and 500 validation images annotated with masks for 19 semantic classes, such as vehicles and pedestrians. The **CamVid** dataset [38] contains 701 images across 11 semantic classes, with 600 used for training and 101 for testing. A subset of the **Apolloscapes** dataset [39], featuring 854 training and 400 test images, provides pixel-level labels for 23 classes like vehicles and pedestrians. The **CARLA_ADV** dataset, generated via the CARLA simulator (version 0.9.13) [40], focuses on adverse weather conditions (e.g., fog, rain) and includes 2,764 training and 1,921 test images, annotated for 23 pixel-level classes such as vehicles and trees.

2) *Evaluation Metrics*: We evaluate MoE-RAM on AD semantic segmentation task using four metrics: **mIoU**, which quantifies the overlap between prediction and ground truth; **mPre**, which measures the accuracy of positive prediction; **mRec**, which evaluates the model's ability to identify relevant instances; and **mF1**, which balances mPre and mRec.

3) *Implementation Details*: For optimization, the Adam optimizer is chosen with Betas values of 0.9 and 0.999, and a weight decay of $1e-4$. All experts within MoE-RAM adopt the ASSP architecture [41] and are trained with a learning rate of $3e-4$. The default configurations of the proposed MoE-RAM include the following hyperparameters: 10 experts, a TopK value of 5, 16 FRL prototypes per expert, a load-balancing weight (λ_{LB}) of 0.01, and a FRL regularization weight (λ_{FRL}) of $1e-4$.

For evaluation, on the one hand, we compare the proposed MoE-RAM with other MoE routing strategies, such as LinearMoE [33], NonlinearMoE [14], and SoftMoE [15]. We should notice that MoE-RAM and these MoE baselines share the same model architecture, where a ViT backbone is used to extract the latent features of inputs, and multiple parallel ASSP experts are integrated into the MoE to serve as the downstream task head. On the other hand, we also compare MoE-RAM with other single-model methods, such as BiSecNetV2 [42], SegNet [43], SegFormer [44], AttaNet [45], HRDA [46], TopFormer [47], and SeaFormer [48].

Notably, the proposed MoE-RAM, all MoE baselines, and all single-model competitors are implemented using the PyTorch framework and trained on two NVIDIA GeForce 4090 GPUs. For MoE-based models, including MoE-RAM, LinearMoE, NonlinearMoE, and SoftMoE, a pretrained ViT backbone is used and frozen, with only the experts (*i.e.*, ASSPs) within the MoE being trained. In contrast, all single-model competitors are trained from scratch using the adopted AD datasets.

TABLE II: Performance comparison of the proposed MoE-RAM against other MoE baselines and single-model approaches for all adopted metrics across multiple AD datasets

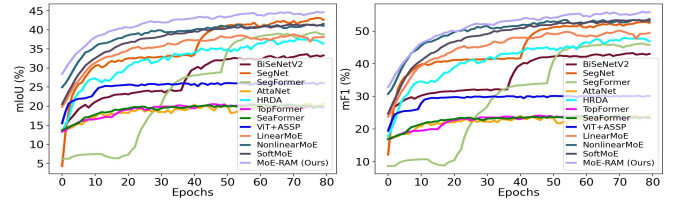
Method	Apolloscapes				CamVid				CARLA_ADV				Cityscapes			
	mIoU	mF1	mPre	mRec	mIoU	mF1	mPre	mRec	mIoU	mF1	mPre	mRec	mIoU	mF1	mPre	mRec
BiSecNetV2	22.92	27.12	-	-	47.89	53.33	-	-	28.80	33.59	-	-	33.63	43.32	-	-
SegNet	21.01	24.60	-	-	46.60	50.18	-	-	31.67	37.15	-	-	43.13	53.87	-	-
SegFormer	-	-	-	-	39.37	46.23	-	-	-	-	-	-	39.37	46.23	-	-
AttaNet	20.89	24.85	26.64	25.67	51.12	58.89	58.83	60.96	28.97	34.46	35.63	34.54	22.96	27.28	26.11	30.87
HRDA	22.19	27.27	34.39	26.94	64.42	75.65	83.66	71.80	34.98	43.10	52.13	40.74	38.89	49.38	64.30	45.80
TopFormer	20.84	24.71	26.37	25.70	48.50	57.02	59.34	57.52	32.32	38.22	41.61	37.20	22.15	26.70	25.48	30.24
SeaFormer	20.58	24.53	25.54	25.28	47.85	56.62	56.22	58.65	28.68	34.24	37.76	33.20	20.51	24.02	23.36	26.85
ViT+ASSP	17.11	21.18	-	-	68.12	77.01	-	-	31.64	37.58	-	-	26.31	30.37	-	-
LinearMoE	21.92	26.76	37.23	26.79	71.07	81.36	84.96	79.74	34.97	42.95	52.48	40.57	39.80	51.53	66.07	47.62
NonLinearMoE	22.32	27.30	37.18	27.03	72.09	82.28	85.66	80.40	35.41	43.50	54.08	41.38	41.74	54.07	65.90	50.15
SoftMoE	22.22	27.11	39.02	26.95	71.54	81.71	85.20	79.54	36.21	44.37	53.39	42.14	42.08	54.45	66.93	49.79
MoE-RAM (Ours)	24.75	28.47	38.35	29.48	72.43	82.89	85.31	80.92	37.97	45.56	55.19	43.39	44.74	55.99	68.30	53.47

B. Main Results and Empirical Analyses

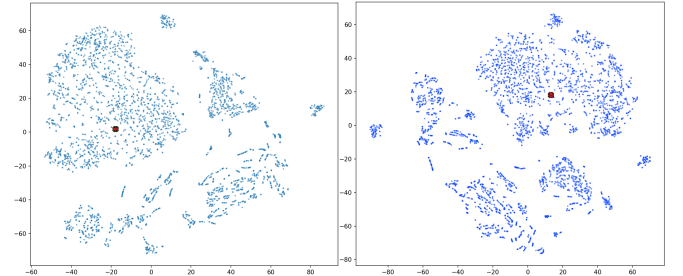
In this section, we present experimental comparison of MoE-RAM against other MoE and single-model baselines, including performance and convergence comparisons.

Table II presents performance comparison of the proposed MoE-RAM against other MoE routing baselines and single-model competitors. The evaluation uses aforementioned four metrics across CamVid, Cityscapes, Apolloscapes, CARLA_ADV datasets. From Table II, we can observe following patterns: (I) The proposed MoE-RAM achieves better performance compared to other baselines for almost all metrics across all datasets, demonstrating its great superiority over other baselines. This suggests that MoE-RAM consistently produces prediction that better match the ground truth. The reason behind it can be attributed to the proposed routing and aggregating mechanisms within MoE-RAM. (II) The limited performance improvement of ViT-based methods (including ViT+ASSP, LinearMoE, NonlinearMoE, SoftMoE, and our MoE-RAM) over single-model architectures can be attributed to the fact that these methods only train the downstream head while keeping the ViT backbone frozen, without fine-tuning it. (III) The performance improvement of MoE methods (including LinearMoE, NonlinearMoE, SoftMoE, and our MoE-RAM) over ViT+ASSP can be attributed to the multiple parallel ASSPs (*i.e.*, experts) in such MoE methods. (IV) The performance improvement of our proposed MoE-RAM over other MoE routing baselines (including LinearMoE, NonlinearMoE, and SoftMoE) can be attributed to our proposed statistic-augmented, decoupled routing strategy (*i.e.*, MoE-RM) and aggregating strategy (*i.e.*, MoE-AM), which suggests their superiority over existing MoE routing strategies.

In addition, we also compare the convergence of the proposed MoE-RAM against other MoE routing baselines and single-model competitors, and the results can be viewed in Fig. 2. From Fig. 2, we can derive the following insights: (I) ViT backbone-based methods (including ViT+ASSP, LinearMoE, NonlinearMoE, SoftMoE, and our MoE-RAM) generally converge faster than single-model approaches. This can be attributed to the pretraining of ViT on a vast number of datasets. (II) The proposed MoE-RAM converges faster than other MoE routing baselines, thanks to the statistic-



(a) mIoU (b) mF1
Fig. 2: Convergence comparison of the proposed MoE-RAM against other MoE baselines and single-model approaches.



(a) T-SNE (b) UMAP
Fig. 3: Relationship visualization between ViT-extracted features and expert-wise FRL prototypes.

augmented, decoupled routing and aggregating strategies.

C. Visualization of the Relationship between Expert-wise FRL Prototypes and ViT-extracted Features

This section visualizes the relationship between ViT-extracted feature representations and the most relevant expert’s FRL prototypes. The results are presented in Fig. 3, which includes two 2D scatter plots generated using t-SNE (Fig. 3a) and UMAP (Fig. 3b), respectively. Each plot overlays sampled ViT token features, represented by smaller points, and FRL prototypes, depicted as larger “X” markers. From Fig. 3, it can be observed that the learned prototypes of the most relevant expert align closely with the majority of the ViT-extracted token features, demonstrating the effectiveness of the proposed expert-wise FRLs.

D. Ablation Study

This section investigates how MoE-RAM-embedded hyperparameters (including the number of experts, the TopK

TABLE III: Performance comparison of cases with different expert numbers within the proposed MoE-RAM

Expert Number	MoE-RAM Remaining Confs	Cityscapes			
		mIoU	mF1	mPre	mRec
7	TopK = 5,	45.45	56.76	71.65	53.22
8	FRL Prototype Number = 16,	45.02	56.08	70.19	53.68
9	$\lambda_{LB} = 0.01$,	44.99	55.82	69.07	53.87
10	$\lambda_{FRL} = 1e-4$	44.74	55.99	68.30	53.47

TABLE IV: Performance comparison of cases with different TopK values in expert routing of MoE-RAM

TopK Value	MoE-RAM Remaining Confs	Cityscapes			
		mIoU	mF1	mPre	mRec
3	Expert Number = 10,	45.85	56.75	69.91	53.69
4	FRL Prototype Number = 16,	45.46	55.47	68.82	53.41
5	$\lambda_{LB} = 0.01$,	44.74	55.99	68.30	53.47
6	$\lambda_{FRL} = 1e-4$	44.33	55.65	67.44	52.48

value, the FRL prototype number, λ_{LB} , and λ_{FRL}) affect the overall performance of MoE-RAM.

1) *The Influence of the Number of Experts on the Overall Performance of MoE-RAM:* Table III showcases the influence of the number of experts on the overall performance of MoE-RAM. From this table, we can find that the case with 7 experts achieves the best performance across almost all metrics. This inspires us that, when the TopK value is fixed, as the number of experts increases, the performance of MoE-RAM declares gradually. In other words, the performance of MoE-RAM is positively related to the proportion of TopK value to the number of experts included in MoE-RAM.

2) *The Effect of the TopK Value on the Overall Performance of MoE-RAM:* Table IV illustrates the effect of the TopK value on the overall performance of MoE-RAM. We can observe from the table that the case with TopK value being 6 performs better than other cases with TopK values ranging from 3 to 5. This shows that when the number of experts within MoE-RAM is fixed, the overall performance of MoE-RAM increases with respect to the TopK value. This further demonstrates that the performance of MoE-RAM is positively correlated with the ratio of the TopK value to the total number of experts included in the proposed MoE-RAM.

3) *The Impact of the FRL Prototype Number on the Overall Performance of MoE-RAM:* Table V demonstrates the impact of the number of experts' FRL prototype for the overall performance of MoE-RAM. From this table, we can observe that the case with an FRL prototype number of 4 outperforms the cases with FRL prototype numbers of 8, 12, and 16, respectively. This suggests that MoE-RAM's overall performance is negatively impacted by an increase in the number of FRL prototypes. Therefore, in practical implementations, it is advisable to set a relatively small number of prototypes in the expert-wise FRL.

4) *The Effect of λ_{LB} on the Overall Performance of MoE-RAM:* Table VI indicates how λ_{LB} imposes the influence on the overall performance of MoE-RAM. We can conclude from this table that the case $\lambda_{LB} = 0.04$ outperforms the case $\lambda_{LB} = 0.00$, indicating that selecting an appropriate value of λ_{LB} can improve the overall performance of MoE-RAM. However, the cases $\lambda_{LB} = 0.02$ and $\lambda_{LB} = 0.08$ perform worse than the case $\lambda_{LB} = 0.00$. This suggests that inap-

TABLE V: Performance comparison of cases with different FRL prototype numbers in the proposed MoE-RAM

FRL Prototype Number	MoE-RAM Remaining Confs	Cityscapes			
		mIoU	mF1	mPre	mRec
4	Expert Number = 10,	45.59	57.35	70.76	53.84
8	TopK = 5,	45.27	56.92	69.16	53.68
12	$\lambda_{LB} = 0.01$,	44.47	55.25	67.99	54.04
16	$\lambda_{FRL} = 1e-4$	44.74	55.99	68.30	53.47

TABLE VI: Performance comparison of cases with different λ_{LB} values in the proposed MoE-RAM

λ_{LB}	MoE-RAM Remaining Confs	Cityscapes			
		mIoU	mF1	mPre	mRec
0.00	Expert Number = 10,	44.23	55.48	71.13	50.82
0.01	TopK = 5,	44.74	55.99	68.30	53.47
0.02	FRL Prototype Number = 16,	43.97	55.19	68.87	52.06
0.04	$\lambda_{FRL} = 1e-4$	45.44	57.17	70.86	53.09
0.08		44.04	55.46	69.30	51.78

TABLE VII: Performance comparison of cases with different λ_{FRL} values in the proposed MoE-RAM

λ_{FRL}	MoE-RAM Remaining Confs	Cityscapes			
		mIoU	mF1	mPre	mRec
0.00	Expert Number = 10,	44.23	55.71	68.62	52.18
1e-4	TopK = 5,	44.74	55.99	68.30	53.47
2e-4	FRL Prototype Number = 16,	44.16	55.47	69.65	52.19
4e-4	$\lambda_{LB} = 0.01$	45.44	57.17	71.17	53.60
8e-4		45.03	56.44	69.93	52.29

propriate setting λ_{LB} can reduce the overall performance of MoE-RAM. In conclusion, proper tuning of λ_{LB} is essential for optimizing the performance of MoE-RAM in practical implementations.

5) *The Impact of λ_{FRL} on the Overall Performance of MoE-RAM:* Table VII compares the results of different λ_{FRL} values on the overall performance of MoE-RAM. We can observe from Table VII that the settings $\lambda_{FRL} = 1e-4$, $\lambda_{FRL} = 4e-4$, and $\lambda_{FRL} = 8e-4$ outperform the setting $\lambda_{FRL} = 0.00$, indicating that selecting an appropriate value of λ_{FRL} can enhance the overall performance of MoE-RAM. However, the case $\lambda_{FRL} = 2e-4$ performs worse than the case $\lambda_{FRL} = 0.00$, suggesting that an inappropriate setting of λ_{FRL} can negatively impact the overall performance of MoE-RAM. In conclusion, careful tuning of λ_{FRL} is crucial for optimizing the performance of MoE-RAM in practical implementations.

V. CONCLUSION

AD scenarios are inherently complex and diverse, presenting significant challenges for a single model to handle varying conditions such as weather, traffic density, and road types. LM-Driven MoE offers a promising solution, where the LM acts as the backbone to extract latent features, while the MoE serves as the downstream head, dynamically selecting and aggregating specialized experts to adapt to different scenarios. However, MoE faces intrinsic challenges like flawed routing strategies and inefficient expert aggregation. To address these limitations, the proposed MoE-RAM incorporates MoE-RM to select the most relevant experts, and integrates MoE-AM to reweight experts' outputs during fusion. Taking AD semantic segmentation as an example

task, extensive experiments on AD datasets demonstrate the superiority of MoE-RAM compared to other MoE routing baselines and conventional single-model methods.

REFERENCES

- [1] Y. Wang and J. Li, "Bilateral knowledge distillation for unsupervised domain adaptation of semantic segmentation," in *2022 IEEE/RSJ International Conference on Intelligent Robots and Systems (IROS)*, 2022, pp. 10 177–10 184.
- [2] N. Kim, T. Son, J. Pakk, C. Lan, W. Zeng, and S. Kwak, "Wedge: Web-image assisted domain generalization for semantic segmentation," in *2023 IEEE International Conference on Robotics and Automation (ICRA)*, 2023, pp. 9281–9288.
- [3] J. Tian, N. C. Mithun, Z. Seymour, H.-P. Chiu, and Z. Kira, "Striking the right balance: Recall loss for semantic segmentation," in *2022 International Conference on Robotics and Automation (ICRA)*, 2022, pp. 5063–5069.
- [4] J. Rückin, F. Magistri, C. Stachniss, and M. Popović, "Semi-supervised active learning for semantic segmentation in unknown environments using informative path planning," *IEEE Robotics and Automation Letters*, vol. 9, no. 3, pp. 2662–2669, 2024.
- [5] Z. Feng, Y. Guo, and Y. Sun, "Cekd: Cross-modal edge-privileged knowledge distillation for semantic scene understanding using only thermal images," *IEEE Robotics and Automation Letters*, vol. 8, no. 4, pp. 2205–2212, 2023.
- [6] W.-B. Kou, Q. Lin, M. Tang, S. Wang, G. Zhu, and Y.-C. Wu, "Fedrc: A rapid-converged hierarchical federated learning framework in street scene semantic understanding," *arXiv preprint arXiv:2407.01103*, 2024.
- [7] W.-B. Kou, Q. Lin, M. Tang, R. Ye, S. Wang, G. Zhu, and Y.-C. Wu, "Fast-convergent and communication-alleviated heterogeneous hierarchical federated learning in autonomous driving," *arXiv preprint arXiv:2409.19560*, 2024.
- [8] W.-B. Kou, G. Zhu, B. Cheng, S. Wang, M. Tang, and Y.-C. Wu, "Fedema: Federated exponential moving averaging with negative entropy regularizer in autonomous driving," *arXiv preprint arXiv:2505.00318*, 2025.
- [9] W.-B. Kou, G. Zhu, Y. Jin, S. Wang, M. Tang, and Y.-C. Wu, "imacs: Intermediate multi-access supervision and regularization in training autonomous driving models," *arXiv preprint arXiv:2505.00404*, 2025.
- [10] S. Mu and S. Lin, "A comprehensive survey of mixture-of-experts: Algorithms, theory, and applications," *arXiv preprint arXiv:2503.07137*, 2025.
- [11] S. Kudugunta, Y. Huang, A. Bapna, M. Krikun, D. Lepikhin, M.-T. Luong, and O. Firat, "Beyond distillation: Task-level mixture-of-experts for efficient inference," *arXiv preprint arXiv:2110.03742*, 2021.
- [12] Y. Li, Y. Lin, L. Zhong, R. Yin, Y. Ji, C. T. Calafate, and C. Wu, "Boosting rare scenario perception in autonomous driving: An adaptive approach with moes and lora," *IEEE Internet of Things Journal*, 2024.
- [13] R. C. Mercurius, E. Ahmadi, S. M. A. Shabestary, and A. Rasouli, "Amend: A mixture of experts framework for long-tailed trajectory prediction," *arXiv preprint arXiv:2402.08698*, 2024.
- [14] H. Nguyen, P. Akbarian, T. Pham, T. Nguyen, S. Zhang, and N. Ho, "Statistical advantages of perturbing cosine router in sparse mixture of experts," *arXiv preprint arXiv:2405.14131*, 2024.
- [15] J. Puigcerver, C. Riquelme, B. Mustafa, and N. Houlsby, "From sparse to soft mixtures of experts," *arXiv preprint arXiv:2308.00951*, 2023.
- [16] J. Achiam, S. Adler, S. Agarwal, L. Ahmad, I. Akkaya, F. L. Aleman, D. Almeida, J. Altenschmidt, S. Altman, S. Anadkat *et al.*, "Gpt-4 technical report," *arXiv preprint arXiv:2303.08774*, 2023.
- [17] H. Touvron, T. Lavril, G. Izacard, X. Martinet, M. Lachaux, T. Lacroix, B. Rozière, N. Goyal, E. Hambro, F. Azhar, A. Rodriguez, A. Joulin, E. Grave, and G. Lample, "Llama: Open and efficient foundation language models," *CoRR*, vol. abs/2302.13971, 2023.
- [18] H. Liu, C. Li, Y. Li, B. Li, Y. Zhang, S. Shen, and Y. J. Lee, "Llava-next: Improved reasoning, ocr, and world knowledge," 2024.
- [19] L. Chen, J. Li, X. Dong, P. Zhang, C. He, J. Wang, F. Zhao, and D. Lin, "Sharegpt4v: Improving large multi-modal models with better captions," *arXiv preprint arXiv:2311.12793*, 2023.
- [20] C. Jia, Y. Yang, Y. Xia, Y.-T. Chen, Z. Parekh, H. Pham, Q. Le, Y.-H. Sung, Z. Li, and T. Duerig, "Scaling up visual and vision-language representation learning with noisy text supervision," in *International conference on machine learning*. PMLR, 2021, pp. 4904–4916.
- [21] A. Radford, J. W. Kim, C. Hallacy, A. Ramesh, G. Goh, S. Agarwal, G. Sastry, A. Askell, P. Mishkin, J. Clark *et al.*, "Learning transferable visual models from natural language supervision," in *International Conference on Machine Learning*. PMLR, 2021, pp. 8748–8763.
- [22] P. Wang, S. Bai, S. Tan, S. Wang, Z. Fan, J. Bai, K. Chen, X. Liu, J. Wang, W. Ge *et al.*, "Qwen2-vl: Enhancing vision-language model's perception of the world at any resolution," *arXiv preprint arXiv:2409.12191*, 2024.
- [23] W.-B. Kou, Q. Lin, M. Tang, S. Xu, R. Ye, Y. Leng, S. Wang, G. Li, Z. Chen, G. Zhu, and Y.-C. Wu, "pfedlvm: A large vision model (lvm)-driven and latent feature-based personalized federated learning framework in autonomous driving," 2024.
- [24] Y. Ma, Y. Cao, J. Sun, M. Pavone, and C. Xiao, "Dolphins: Multimodal language model for driving," in *European Conference on Computer Vision*, 2024.
- [25] X. Tian, J. Gu, B. Li, Y. Liu, Y. Wang, Z. Zhao, K. Zhan, P. Jia, X. Lang, and H. Zhao, "Drivevlm: The convergence of autonomous driving and large vision-language models," *arXiv preprint arXiv:2402.12289*, 2024.
- [26] M. Nie, R. Peng, C. Wang, X. Cai, J. Han, H. Xu, and L. Zhang, "Reason2drive: Towards interpretable and chain-based reasoning for autonomous driving," in *European Conference on Computer Vision*. Springer, 2024.
- [27] Z. Xu, Y. Zhang, E. Xie, Z. Zhao, Y. Guo, K.-Y. K. Wong, Z. Li, and H. Zhao, "Drivegpt4: Interpretable end-to-end autonomous driving via large language model," *IEEE Robotics and Automation Letters*, 2024.
- [28] H. Shao, Y. Hu, L. Wang, G. Song, S. L. Waslander, Y. Liu, and H. Li, "Lmdrive: Closed-loop end-to-end driving with large language models," in *Conference on Computer Vision and Pattern Recognition*, 2024.
- [29] I. Kim, J. Lee, and D. Kim, "Learning mixture of domain-specific experts via disentangled factors for autonomous driving," in *Proceedings of the AAAI Conference on Artificial Intelligence*, vol. 36, no. 1, 2022, pp. 1148–1156.
- [30] S. Pini, C. S. Perone, A. Ahuja, A. S. R. Ferreira, M. Niendorf, and S. Zagoruyko, "Safe real-world autonomous driving by learning to predict and plan with a mixture of experts," *arXiv preprint arXiv:2211.02131*, 2022.
- [31] Q. Sun, H. Wang, J. Zhan, F. Nie, X. Wen, L. Xu, K. Zhan, P. Jia, X. Lang, and H. Zhao, "Generalizing motion planners with mixture of experts for autonomous driving," *arXiv preprint arXiv:2410.15774*, 2024.
- [32] C. Riquelme, J. Puigcerver, B. Mustafa, M. Neumann, R. Jenatton, A. Susano Pinto, D. Keysers, and N. Houlsby, "Scaling vision with sparse mixture of experts," *Advances in Neural Information Processing Systems*, vol. 34, pp. 8583–8595, 2021.
- [33] Z. Fan, R. Sarkar, Z. Jiang, T. Chen, K. Zou, Y. Cheng, C. Hao, Z. Wang *et al.*, "M³vit: Mixture-of-experts vision transformer for efficient multi-task learning with model-accelerator co-design," *Advances in Neural Information Processing Systems*, vol. 35, pp. 28 441–28 457, 2022.
- [34] B. Li, Y. Shen, J. Yang, Y. Wang, J. Ren, T. Che, J. Zhang, and Z. Liu, "Sparse mixture-of-experts are domain generalizable learners," *arXiv preprint arXiv:2206.04046*, 2022.
- [35] K.-C. Wang, D. Ostashev, Y. Fang, S. Tulyakov, and K. Aberman, "Moa: Mixture-of-attention for subject-context disentanglement in personalized image generation," in *SIGGRAPH Asia 2024 Conference Papers*, 2024, pp. 1–12.
- [36] A. Dosovitskiy, L. Beyer, A. Kolesnikov, D. Weissenborn, X. Zhai, T. Unterthiner, M. Dehghani, M. Minderer, G. Heigold, S. Gelly *et al.*, "An image is worth 16x16 words: Transformers for image recognition at scale," *arXiv preprint arXiv:2010.11929*, 2020.
- [37] M. Cordts, M. Omran, S. Ramos, T. Rehfeld, M. Enzweiler, R. Benenson, U. Franke, S. Roth, and B. Schiele, "The cityscapes dataset for semantic urban scene understanding," in *Proc. of the IEEE Conference on Computer Vision and Pattern Recognition (CVPR)*, 2016.
- [38] G. J. Brostow, J. Shotton, J. Fauqueur, and R. Cipolla, "Segmentation and recognition using structure from motion point clouds," in *Computer Vision—ECCV 2008: 10th European Conference on Computer Vision, Marseille, France, October 12–18, 2008, Proceedings, Part I 10*. Springer, 2008, pp. 44–57.
- [39] P. Wang, X. Huang, X. Cheng, D. Zhou, Q. Geng, and R. Yang, "The apolloscape open dataset for autonomous driving and its application," *IEEE transactions on pattern analysis and machine intelligence*, 2019.

- [40] A. Dosovitskiy, G. Ros, F. Codevilla, A. Lopez, and V. Koltun, "Carla: An open urban driving simulator," in *Proceedings of The 1st Annual Conference on Robot Learning*, 2017, pp. 1–16.
- [41] L.-C. Chen, G. Papandreou, F. Schroff, and H. Adam, "Rethinking atrous convolution for semantic image segmentation," *arXiv preprint arXiv:1706.05587*, 2017.
- [42] C. Yu, C. Gao, J. Wang, G. Yu, C. Shen, and N. Sang, "Bisenet v2: Bilateral network with guided aggregation for real-time semantic segmentation," *International Journal of Computer Vision*, vol. 129, pp. 3051–3068, 2021.
- [43] V. Badrinarayanan, A. Kendall, and R. Cipolla, "Segnet: A deep convolutional encoder-decoder architecture for image segmentation," *IEEE transactions on pattern analysis and machine intelligence*, vol. 39, no. 12, pp. 2481–2495, 2017.
- [44] E. Xie, W. Wang, Z. Yu, A. Anandkumar, J. M. Alvarez, and P. Luo, "Segformer: Simple and efficient design for semantic segmentation with transformers," in *Neural Information Processing Systems (NeurIPS)*, 2021.
- [45] Q. Song, K. Mei, and R. Huang, "Attanet: Attention-augmented network for fast and accurate scene parsing," in *Proceedings of the AAAI conference on artificial intelligence*, vol. 35, no. 3, 2021, pp. 2567–2575.
- [46] L. Hoyer, D.-X. Dai, and L. Van Gool, "Domain adaptive and generalizable network architectures and training strategies for semantic image segmentation," *IEEE Transactions on Pattern Analysis and Machine Intelligence*, 2023.
- [47] W. Zhang, Z. Huang, G. Luo, T. Chen, X. Wang, W. Liu, G. Yu, and C. Shen, "Topformer: Token pyramid transformer for mobile semantic segmentation," in *Proceedings of the IEEE/CVF Conference on Computer Vision and Pattern Recognition*, 2022, pp. 12 083–12 093.
- [48] Q. Wan, Z. Huang, J. Lu, Y. Gang, and L. Zhang, "Seaformer: Squeeze-enhanced axial transformer for mobile semantic segmentation," in *The eleventh international conference on learning representations*, 2023.